Non-exponential tunneling ionization probability distribution as a function of different laser beam profiles

T. B. Miladinović
University of Kragujevac, Institute for Information Technologies, Department of Sciences, Jovana Cvijića bb, 34000 Kragujevac, Serbia,
e-mail: tanja.miladinovic@uni.kg.ac.rs

N. Danilović
University of Kragujevac, Faculty of Science, Department of Physics, Radoja Domanovića 12, 34000 Kragujevac, Serbia.

M. Z. Jeremić
University Clinical Center Kragujevac, Department of Nuclear Medicine, Zmaj Jovina 30, 34000 Kragujevac, Serbia.

Received 6 October 2021; accepted 17 November 2021

In this paper, we discussed the probability distribution of exponential and non-exponential tunneling ionization of atoms, taking into account that the tunneling is not instantaneous, but requires a very short time interval. We also investigated how different laser beam profiles affected the probability distribution. These physical situations were analyzed for the valence electron of a potassium atom exposed to a strong laser field in a wide range of intensities ($10^{12} - 10^{15}$ W/cm^2). We used the ADK theory formalism to compute probability distributions. The results demonstrate that the probability distribution in the non-exponential mode has a significantly lower value than in the exponential mode, calculated under the same conditions. We showed that various laser beam profiles on these probability distributions produce different tunneling time intervals.

Keywords: Non-exponential decay; tunneling ionization probability; tunneling time; laser beam profiles.

DOI: https://doi.org/10.31349/RevMexFis.68.040401

1. Introduction

Today it is possible to get laser pulses of high intensities even to relativistic orders, with their duration lasting less than a femtosecond. That is why studying the tunneling ionization process, which occurs when a laser interacts with matter, is much easier. This analysis was impossible before the 1980s. Experimental confirmation of the existence of this process [1] opened a completely new chapter in quantum physics. It enabled the approach to many important scientific issues from a totally different perspective, such as radioactive decay [2, 3], the scanning tunneling microscope (STM) that gives information about surface topography [4, 5]; in the area of public health and safety, as an innovative concept for nanostructure-based gas ionization sensors [6–8]; a technique called "tunneling ionization with a perturbation for the time-domain observation of an electric field" (TIPTOE) was developed. Using TIPTOE, the temporal profile of an input pulse can be determined by modulation of the ionization yield using an appropriate reconstruction algorithm [9, 10].

In a well-defined combination of strong intensity and a correspondingly low frequency of the laser field, in the infrared or optical domain, electron tunneling occurs through a potential barrier, which is impenetrable in classical mechanics. The laser electric field suppresses the Coulomb potential and thus forms a barrier through which the electron can tunnel. To describe the tunneling process, scientists have developed models and theories. Just a few of them will be mentioned. Starting from the Schrödinger equation for a hydrogen atom in a uniform electric field, Landau and Lifshitz determined the ionization probability (per unit of time) [11]. In 1965. Keldysh wrote a paper whose essence was to express rate as a sum of multiphoton processes, given as a total ionization rate [12]. He derived a relatively complex formula, but using the function: $\gamma = \omega\sqrt{2m_e I_p}/(eF)$, it can be divided into two independent equations related to two types of ionization, tunnel and multiphoton. This function is called the Keldysh parameter, where: ω, F and I_p interpret the frequency of the external field, laser-field strength and ionization potential, respectively, e and m_e are the charge and mass of the electron, respectively. It is generally accepted that ionization processes can be separated by the Keldysh parameter, in the following way: when the Keldysh parameter has a value $\gamma \ll 1$, ionization occurs in the tunnel mode, while in the case of $\gamma \gg 1$, in the multiphoton mode. The first experiments satisfied Keldysh's parameter condition. Later experiments showed that these limits do not have to be strictly adhered to [13, 14]. Theories that directly rely on Keldysh's theory are PPT (Perelomov, Popov and Terent'ev) [15] and ADK (Ammosov, Delone and Krainov) [16]. These theories have adapted and improved Keldish's theory and can be applied on hydrogen atoms and extended to more complex atoms and molecular systems. In ADK theory the regions, in which the ionized electron interacts with the parent ion and

with the electric field, can be separated. The electron bound in the atom moves under the influence of the atomic forces, and the external field does not influence its motion and vice versa. The ionized electron moves only under the influence of the external field, in which the energy of one photon is smaller than the ionization potential $\omega \ll I_p$ and the field strength is smaller compared to the strength of the atomic field $F \ll F_a$, $F_a = 5.14 \times 10^9$ V/cm. Under these conditions, the atom is treated quantum mechanically while the electromagnetic field is classical. However, in both cases, there are deviations from the given rules. In the case of an electromagnetic field, the term photon is used, while in the case of atoms, a quasi-classical approximation is used, *i.e.* states with a large quantum number n are observed. Ammosov, Delone and Krainov in their paper replaced the quantum numbers n, l by their effective values $n^* = Z/\sqrt{2I_p}$ and $l^* = n_0^* - 1$, where Z is a charge of the ionized atom, while n_0^* is the smallest value of the effective quantum number n^*.

The resulting formula given by the ADK theory describes the tunnelling process in which an unstable system decays according to the exponential law. The probability of survival of such a system decreases exponentially with time t. This method of calculating the tunnel ionization rate has become accepted and widely used, but tunneling can also be analyzed in a non-exponential mode [17, 18]. To mention briefly, in the 1920s, the law of decay in the exponential form was established [19, 20]. In the 1950s Khalfin [21] assumed the existence of decay, which can be described by a non-exponential law, and his assumptions were proved experimentally [22, 23]. Time dependence of non-exponential decay is in the form $t^{-3/2}$, but Nicolaides and Beck [24] suggested in their paper that this dependence could be $\sim t^{-1}$. For non-exponential decay in a many-particle system that takes place over a longer period. This dependence is also possible in the form t^{-N}, where the quantity N is proportional to the number of particles and depends on the quantum Bose-Einstein or Fermi-Dirac statistics of these particles. There are several approaches how to determine the tunneling time. One of them is Keldysh's [12], in which tunneling through a barrier is instantaneous and doesn't take a finite time. Buttiker and Landauer considered time to be imaginary because it is thought that a breakdown of a wave function is below the barrier [25]. One of the concepts is that the tunneling time is viewed as an average value, not as a quantity that is strictly determined. Using this way of approaching the problem, the Feynman path integral (FPI) was obtained [26, 27], which can be presented as a process of averaging using the tunneling time of probability amplitude. The development of science enables us to solve this dilemma experimentally. Now it is possible to determine the real tunneling time using attoclock measurements in a wider range of laser field intensities [28]. For a more detailed analysis of the tunnel ionization process and calculation of the ionization probability distribution of ejected electrons, it's important to take into account the spatial distribution of a laser beam profile when optimizing the experimental setup. Laser systems can operate with near-Gaussian beams or non-Gaussian beams. The most commonly used models of laser beam shaped profiles, in physics as well as in other branches of sciences, are Gaussian [29,30], Super-Gaussian (SG) (flat-top beams where a beam exhibits a nearly constant irradiance over its beam width) [31], Hermite-Gaussian (HG) (rectangular) [32–34], cylindrical and are called Laguerre-Gaussian (LG) [35, 36], as well as Lorentzian [37]. Experimentally it is possible to achieve a transition from a spot-like profile of the laser beam to a doughnut shape, and vice versa [38–40]. The processes that take place under the influence of the laser field must be discussed theoretically by including different spatial distributions of the laser beam, from fundamental modes (Lorentzian and Gaussian) to higher-order beam modes (SG, HG, LG). This paper report results obtained by calculating and estimating the effects of different laser beam profiles on ionization probability distributions in a wide range of laser intensities for the specific wavelength in the infrared domain, when the electron tunneling time is in the range of $t = (1 - 800)$ as. Potassium was chosen as the target atom exposed in a linearly polarized laser field. This model is applicable in a non-relativistic regime, for laser intensities less than 10^{18} W/cm^2. It could be extended to a relativistic regime for much higher intensities, with the inclusion of required relativistic corrections, but this would be out of the scope of this paper. Research in the fields of ultrahigh laser intensities exceeding 10^{20} W/cm^2 would allow studying multiple tunneling ionization of heavy atoms [41, 42].

The structure of our paper is the following. After the introduction, the theoretical background is presented in Sec. 2, followed by a presentation of the results and discussion (Sec. 3) where the probability distribution in exponential and non-exponential modes was calculated. In Sec. 4 we gave our conclusions. A complete description of the systems of probability equations, as well as all the parameters needed for their implementation, are given in atomic units ($|e| = m_e = \hbar = 1$).

2. Theoretical background

An unstable system has multiple ways of decaying: spontaneous decay, tunneling alpha decay of atomic nuclei, single-photon ionization of atoms, etc. The basic formulas used to describe each of the decay processes are [43]:

$$a(t) = \langle S|e^{-iHt}|S\rangle, \tag{1}$$

$$P(t) = |a(t)|^2, \tag{2}$$

where $|S\rangle$ is the state vector, H is the Hamiltonian of an unstable system, while *a(t)* and *P(t)* is the decay survival probability amplitude and the survival probability, respectively. The unstable state $|S\rangle$ is not an eigenstate of the Hamiltonian H, and the energy distribution of this state can be defined as:

$$a(t) = \int_{-\infty}^{\infty} d_s(E) e^{-iEt} \mathrm{d}E, \tag{3}$$

where the energy normalization condition holds:

$$\int_{-\infty}^{\infty} d_s(E) \mathrm{d}E = 1. \tag{4}$$

In order to discuss the probability distribution of exponential and non-exponential tunneling ionization of atoms exposed to an intense laser field, it is necessary to define the probability amplitude for both of these mechanisms.

2.1. Exponential decay

The energy distribution of an ejected electron of the exponential decay, with respect to mean electron energy ϵ, is given by the Breit-Wigner distribution [44]:

$$d_s(E) = \frac{1}{2\pi} \frac{\Gamma(E)}{\left((E-\epsilon)^2 + \frac{\Gamma(\epsilon)^2}{4}\right)}, \tag{5}$$

where $\Gamma(E)$ is the decay width. A detailed derivation of this equation can be found in Ref. [45]. The first step in deriving the probability amplitude is to apply the Fourier transform using a complex integral:

$$f(t) = \int_{-\infty}^{\infty} \frac{1}{2\pi} F(\omega) e^{-i\omega t} \mathrm{d}\omega. \tag{6}$$

Function $F(\omega)$ has two simple poles at $\omega = \epsilon \pm i(\Gamma(\epsilon)/2)$. The integral at pole $\omega = \epsilon + i(\Gamma(\epsilon)/2)$ diverges and correspond to an unphysical state; therefore we account only for the contribution from the simple pole located at $\omega = \epsilon - i(\Gamma(\epsilon)/2)$ in order to obtain an exponentially decaying state.

By the residue theorem:

$$\int_{\text{arc}} F(\omega)\mathrm{d}\omega - \int_{-\infty}^{\infty} F(\omega)\mathrm{d}\omega = 2\pi i \mathrm{Res}_{\omega=\epsilon-i(\Gamma(\epsilon)/2)} F(\omega). \tag{7}$$

The first integral tends to zero,

$$\int_{\text{arc}} F(\omega)\mathrm{d}\omega \to 0.$$

The notation arc means arc length and represents the distance between two points along a section of a curve. Eq. (5) can be written in the following form:

$$d_s(E) = \frac{1}{2\pi} \frac{2(\frac{\Gamma(\epsilon)}{2})}{\left(\frac{\Gamma(\epsilon)}{2}\right)^2 + (E-\epsilon)^2} = \frac{1}{2\pi} \left(\frac{1}{\frac{\Gamma(\epsilon)}{2} + i(E-\epsilon)} + \frac{1}{\frac{\Gamma(\epsilon)}{2} - i(E-\epsilon)} \right), \tag{8}$$

by applying the residual theorem Eq. (7) and after several mathematical transformations the Breit-Wigner probability amplitude can be obtained:

$$a_0^{(1)}(t) = -i\Gamma(\epsilon) \Bigg[\int_{-\infty}^{\infty} \frac{e^{-iEt}}{\frac{\Gamma(\epsilon)}{2} + i(E-\epsilon)} \mathrm{d}E + \int_{-\infty}^{\infty} \frac{e^{-iEt}}{\frac{\Gamma(\epsilon)}{2} - i(E-\epsilon)} \mathrm{d}E \Bigg]. \tag{9}$$

A suitable simple pole at $E = \epsilon - i(\Gamma(\epsilon)/2)$ in Eq. (9) provides:

$$a_0^{(1)}(t) = -i \int_{-\infty}^{\infty} e^{-i(\epsilon - i(\Gamma(\epsilon)/2)t} \mathrm{d}(\epsilon - i(\Gamma(\epsilon)/2), \tag{10}$$

which leads to the formula for the probability amplitude of the initial state:

$$a_0^{(1)}(t) = e^{-i\epsilon t - \frac{\Gamma(\epsilon)}{2}t}. \tag{11}$$

The decay width $\Gamma = 1/\tau$ is the inverse of a lifetime, which is the initial decay rate, and can be measured by fitting the counting rate of decay products to the exponential law:

$$\frac{1}{N}\frac{dN(t)}{dt} \propto \Gamma e^{-\Gamma t}, \tag{12}$$

where $dN(t)$ is the number of decay products registered in the detector during the time interval dt. In the case of the tunneling ionization of an atom in a strong low-frequency laser field the width $\Gamma(E)$ can be represented by the equation [18]:

$$\Gamma(E) = 4\sqrt{\frac{3\gamma}{\pi\omega\sqrt{2I_p}}} \exp\left(-\frac{2(1-E\gamma^2)}{3F}\right), \tag{13}$$

where E is the kinetic energy and has values greater than zero, $E > 0$ [15]. The probability amplitude is interpreted as the possibility of the appearance of a particle (in our case an electron) at the moment t when it's mean kinetic energy is ϵ. The probability amplitudes are complex numbers. The corresponding probability is proportional to the modulus squared of the probability amplitude, which, unlike the amplitude, is a positive real number. The square of the module of Eq. (11) gives:

$$P^{(1)}_{\text{Exponential}} = \exp[-\Gamma(E)t], \tag{14}$$

where the mean electron energy $E = \epsilon$ corresponds to the average kinetic energy of the ejected electron that oscillates in the electric field and it is equal to the ponderomotive potential. The ponderomotive potential for a linearly polarized laser field has the form $\epsilon = U_p = F^2/(4\omega^2)$ [46, 47]. Using the expression for mean electron energy ϵ and substituting expression Eq. (13) into Eq. (14) probability is defined as:

$$P^{(1)}_{\text{Exponential}}(F,t) = \exp\left(-\left[A\exp\left\{-\frac{2}{3F} - \frac{F\gamma^2}{6\omega^2}\right\}\right]t\right), \tag{15}$$

where is $A = 4\sqrt{3\gamma/(\pi\omega\sqrt{2I_p})}$.

2.2. Non-exponential decay

To get a basic insight into the mechanism of non-exponential ionization of the tunnel, it is required to calculate the appropriate probability amplitude as a function of time. Starting from Eqs. (5) and (6) the following is obtained [48]:

$$a_0^{(2)}(t) = \frac{1}{2\pi}\int_0^\infty \frac{e^{-ixt}\Gamma(-x)}{(x+\epsilon)^2+\frac{\Gamma(-x)^2}{4}}\mathrm{d}x. \tag{16}$$

Choosing a negative imaginary axis is useful for calculating a long time limit. The analysis will remain unchanged when using this integration contour, as long as the contour closes the physically relevant poles near the positive real axis. After implementing the replacement $y = xt$, the equation above becomes:

$$a_0^{(2)}(t) = \frac{1}{2\pi t}\int_0^\infty \frac{e^{-iy}\Gamma(-y/t)}{(y/t+\epsilon)^2+\frac{\Gamma(-y/t)^2}{4}}\mathrm{d}y. \tag{17}$$

Knowing that at $t \to \infty$ the non-exponential decay is determined by small values of $E \to 0$, the denominator in Eq. (17) becomes equal to ϵ^2:

$$a_0^{(2)}(t) = \frac{1}{2\pi\epsilon^2 t}\int_0^\infty e^{-iy}\Gamma(-y/t)\mathrm{d}y. \tag{18}$$

This time limit determines the behavior of near zero, that $\Gamma(-y/t) = \Gamma(0)$ [48,49]:

$$a_0^{(2)}(t) = -\frac{i\Gamma(0)}{2\pi\epsilon^2 t}. \tag{19}$$

In accordance with Eq. (13), the non-exponential decay width is obtained:

$$\Gamma(0) = 4\sqrt{\frac{3\gamma}{\pi\omega\sqrt{2I_p}}}\exp\left(-\frac{2}{3F}\right). \tag{20}$$

This derivation leads to a finite expression for probability in a non-exponential mode:

$$P^{(2)}_{\text{Non-exponential}} = \left(-\frac{\Gamma(0)}{2\pi}\right)^2 \frac{1}{\epsilon^4 t^2}, \tag{21}$$

$$P^{(2)}_{\text{Non-exponential}}(F,t) = \left(A\exp\left[-\frac{2}{3F}\right]\right)^2 \frac{4\omega^4}{(\pi F^2)^2 t^2}. \tag{22}$$

In the tunnel ionization regime, the total probability can be viewed as a function of $P(F,t)$, which maps values into real numbers over the range of [0,1]. A detailed theoretical analysis of the ionization probability gives us an advantage in better understanding of the experimental data. Experimental determination of absolute ionization probabilities is complicated because ionization of atoms in strong laser fields depends on various experimental setups: target density, excited state fraction, incoming photon flux, detector efficiency and relative spatial alignment of the target and laser pulse [50,51]. Therefore, we tested the influence of different beam profiles on exponential and non-exponential probability distributions.

The Gaussian (G) beam profile was the first we paid attention to. The electric field for this beam profile can be expressed as [30, 31]:

$$F_G = F_0\exp\left(-\left[\frac{r}{\omega(z)}\right]^2\right), \tag{23}$$

where r^2 is the distance from the centre of the beam, $\omega(z) = \omega_0\sqrt{1+(z/z_0)^2}$ is the Gaussian width, ω_0 is the Gaussian beam waist, z_0 is the Rayleigh length. A Gaussian-shaped laser beam does not necessarily have to be parabolic; it also can be a flat-top beam *i.e.* higher-order Gaussian (Super-Gaussian). A Super Gaussian (SG) electric field is given by [52]:

$$F_{SG} = F_0\exp\left(-\left[\frac{r}{\omega(z)}\right]^n\right), \tag{24}$$

n represents the order/index of the Super-Gaussian beam, and it's value is $n > 2$. The case $n = 2$ corresponds to the basic Gaussian profile. It is shown that the Super-Gaussian beam of the higher index and smaller beam width can produce much stronger radiation compared to the Gaussian beam [52]. By differentiating the fundamental Gaussian mode, higher-order beams like Hermite-Gaussian and Laguerre-Gaussian with complex arguments can be obtained. These calculations can be generalized to deriving a whole family of Hermite-Gaussian (HG) and Laguerre-Gaussian (LG) modes, including also those with real arguments [53, 54]. Field intensity distributions of higher-order HG mode laser beams and the amplitude of the electric field are given in literature [55, 56]. For this research the Hermite-Gaussian beam of the first order was used:

$$F_{HG}(z) = \frac{\omega_0}{\omega(z)^2}\sqrt{\frac{8x^4}{\omega_0^2\omega(z)^2} - \frac{8x^2}{\omega(z)^2} + 2} \times \exp\left(\frac{1}{2} - \left[\frac{r}{\omega(z)}\right]^2\right). \tag{25}$$

The Hermite-Gaussian mode is closely related to the Laguerre-Gaussian mode, and some research requires conversion of the HG into the LG mode and vice versa. The way this can be performed is given in literature [57]. The behavior of tunneling probabilities under the influence of a LG(0,1)* spiral phase mode was also analyzed. The electric field for a linearly polarized laser light with this beam profile is given by [58]:

$$F_{LG(SP)} = F_0\sqrt{\frac{2r_a^2}{\omega_0^2}}\exp\left(-\frac{r_a^2}{\omega_0^2}\right)\cos\phi, \tag{26}$$

where $r_a(\phi) = ae^{k_a\phi}$ is the polar equation, a and k_a are constants, while ϕ is the azimuthal angle. More about LG beams can be seen in Refs. [59–61]. In experiments, high laser intensities are involved. It has been shown that the transverse intensity profile is not always described well by a Gaussian distribution [62,63] and that Lorentzian's (L) distribution would be more appropriate [40, 64, 65]. A Lorentzian electric

field distribution function was propounded in work of Shealy *et al.* [66]:

$$F_L = \frac{F_0}{1+\left(\frac{r}{\omega(z)}\right)^2} \,. \tag{27}$$

Experiments in the attosecond domain indicated that the tunneling time is much shorter than predicted by theories [67, 68]. The presented laser beam profiles in combination with controlled light pulses lasting attoseconds $(10^{-18}\mathrm{s})$, made it possible to observe what happens during ionization, providing the possibility of a detailed analysis of the process.

3. Results and discussion

The behavior of an atom located in the external electromagnetic field, directed along the z axis, can be conveniently investigated in parabolic coordinates: $\xi = r + z$, $\eta = r - z$, $\phi = \arctan(y/z)$, where ϕ is the azimuthal angle, $\phi \in [0, 2\pi]$, $\xi, \eta \in [0, \infty)$. Conversely in Cartesian coordinates $x = \sqrt{\xi\eta}\cos\phi$, $y = \sqrt{\xi\eta}\sin\phi$, $z = (\xi - \eta)/2$, $r = \sqrt{x^2 + y^2 + z^2} \Leftrightarrow r = (\xi + \eta)/2$. Therefore, all the quantities given in Cartesian coordinates, in the equations above, were converted into parabolic coordinates before the analysis started.

The potential barrier through which the electron tunnels is along the η coordinate in the direction $z \to -\infty$, where the η coordinate has higher values. The exit point is determined by $\eta_{exit} \cong 1/F$ in the range $1 \ll \eta \ll \eta_{exit}$ [11, 69]. The laser field strength for linearly polarized light in atomic units is approximately equal to $\sim 5.4 \times 10^{-9}\sqrt{I}$, and within a broad intensity range $(10^{12} - 10^{15})$ W/cm^2, exponential and non-exponential tunneling was observed. These intensities correspond to the values of η coordinates in the range $6 - 185$ a.u.. The investigation was performed when the exit point was $\eta = 10$. It is possible that the tunnel exit point is located in this region for the laser intensity $I \sim 3 \times 10^{14}$ W/cm^2. Calculations were done for an intense infrared Ti: sapphire laser pulse with wavelength $\lambda = 800$ nm (15117.2 a.u.), beam waist of $\omega_0 = 4$ mm (7.559×10^7 a.u.) [70, 71] and photon energy $\omega = 0.05696$ a.u. It should be emphasized that the beam waist can be in a wide range of values, from micrometers $(3 - 60)$ μm to millimeters $(15 - 30)$ mm. Higher-order beam modes correspond to the narrower beam waist and ω_0 has to be adapted. The target to which this beam is directed is the potassium atom with the ionization potential of valence electron of $I_p = 4.3406$ eV (0.1595 a.u.). The value of the Keldysh parameter is $\gamma = 0.1$, which is in the range of values given by the condition $\gamma \ll 1$ that defines the domain of tunnel ionization.

To calculate the probability for a Laguerre-Gaussian beam shape, it was necessary to define the values of the parameters that appear in Eq. (26). $r_a(\phi) = ae^{k_a\phi}$ is the logarithmic function when r_a has a value in μm range, parameter a is equal to $a = 0.57$ (1.08×10^4 a.u.). ϕ is azimuthal angle lies in interval $[-180°, 180°]$. Angle θ defines spiral geometry $\theta \in [-90°, 90°]$. Using this angle, the constant k_a can be determined. $k_a = \tan\theta$ which for $\theta = 22.5°$ and $\theta = 45°$ are $k_a = 0.414$ and $k_a = 1.0$, respectively. As said above, higher-order beams produce a much smaller focused spot than a conventional beam and the diameter is fixed to the value 3 μm (5.7×10^4 a.u.) [72].

3.1. Exponential mode

The exponential probability distribution is given Eq. (15) when a field strength of a laser pulse is approximately equal to the root of the field intensity and without a defined spatial distribution $(F \sim \sqrt{I})$, hereinafter referred to as basic. The behavior of the probability distribution is observed in a wide range of laser field intensity and tunneling time interval $(1 - 800)$ as, which is sufficiently long enough for an ionization event to occur (as confirmed in experiments [28, 73]). It should be emphasized that the Figures given in the text are computed for laser intensity in the interval $(10^{12} - 5 \times 10^{15})$ W/cm^2. However, in the laser intensity

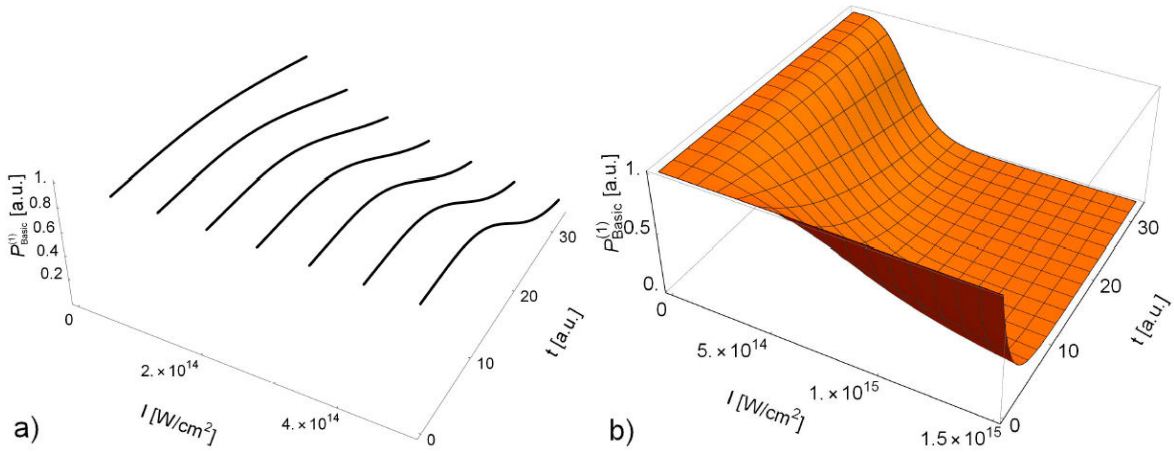

FIGURE 1. Exponential probability distribution $P^{(1)}_{Basic}$ for the tunneling time range $t = (1 - 800)$ as *i.e.* $t = (0.041 - 33.073)$ a.u. (a) in the interval of laser intensities $I = (10^{14} - 5 \times 10^{14})\mathrm{W/cm}^2$, (b) $I = (10^{14} - 1.5 \times 10^{15})$ W/cm^2.

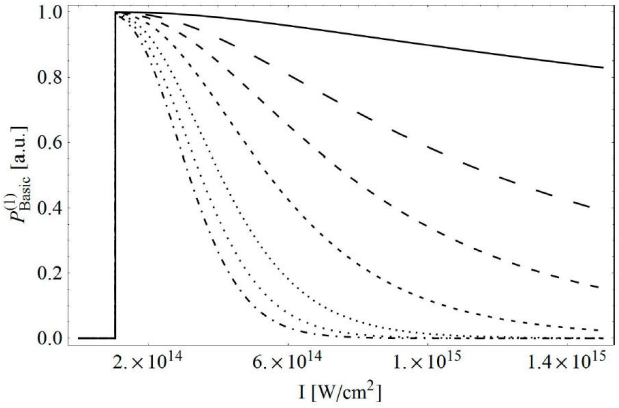

FIGURE 2. Exponential probability distribution $P^{(1)}_{\text{Basic}}$, for the laser intensity range $I = (10^{14} - 1.5 \times 10^{15})$ W/cm^2. Each probability curve corresponds to an integer value of attoseconds of tunneling time $t_1 = 1$ as (solid line), $t_2 = 50$ as (large dashed line), $t_3 = 100$ as (medium dashed line), $t_4 = 200$ as (small dashed line), $t_5 = 400$ as (tiny dashed line), $t_6 = 600$ as (dotted line), $t_7 = 800$ as (dot-dashed line).

range of $(10^{12} - 10^{13})$ W/cm^2 the probability is negligible, so in Figs. 1-10 we showed the probability distribution for the laser intensity range of $(10^{14} - 10^{15})$ W/cm^2.

$P^{(1)}_{\text{Basic}}$ 2D curves, plotted into a 3D coordinate system, provide the opportunity to quite clearly notice the dependence of the exponential probability distribution on the tunneling time for the specific values of the laser field intensities: $(0.8 \times 10^{13}, 1.4 \times 10^{14}, 2.0 \times 10^{14}, 2.6 \times 10^{14}, 3.2 \times 10^{14}, 3.8 \times 10^{14}, 4.4 \times 10^{14})$ W/cm^2 (Fig. 1a). At the field intensity of $\sim 10^{14}$ W/cm^2, no matter how long the tunneling time is, the distribution of the electron ionization probability changes very little, while with increasing field intensity, the maximum probabilities are more pronounced. It can be assumed that an electron in a very short time interval receives an amount of energy sufficient to pass through a potential barrier so that the tunneling time with increasing intensity becomes shorter.

Dependences of the ionization process for any values of tunneling time in an extended range of intensities $I = (10^{12} - 1.5 \times 10^{15})$ W/cm^2 can be estimated from the 3D surface (Fig. 1b). In very intensive fields, the exponential probability distribution of the tunneling time reaches a maximum for $t \sim 1$ as. As the laser field intensity increases, the range of values of the tunneling time narrows. The probability distribution $P^{(1)}_{\text{Basic}}$ as a function of laser field intensity for the fixed integer value of attosecond tunneling time is shown in Fig. 2. The probability sharply increases with the increase of laser intensity for all observed tunneling time values, then reaches a maximum at the same field intensity 0.2×10^{14} W/cm^2 and then with a further increase of intensity decreases slightly in different ways. The longer the expected tunneling time is, the faster the probability decreases.

For the tunneling time of 1as (0.041 a.u.), a maximum probability value is $P^{(1)}_{\text{Basic}} = 1$ or $P^{(1)}_{\text{Basic}} \approx 1$ for almost all the field intensities ranges. With the tunneling time increase up to several hundred attoseconds and with increasing laser intensity, the probability decreases, which corresponds to the physical picture that the electron requires real time to tunnel through the barrier, in fact, as the interaction time with the electron shortens, the probability that the electron will completely tunnel through the barrier becomes greater [74]. The probability reaches a maximum at a precisely defined laser intensity and then decreases monotonically, which is the effect of atom stabilization in the superintense field [75].

By including Eqs. (23), (24), and Eq. (27) in Eq. (15) we obtained probability distributions $P^{(1)}_G$, $P^{(1)}_{SG}$, $P^{(1)}_L$. From Fig. 3a) and 3b) one can see that these probabilities behave in the same manner. At the fixed laser intensity, the probabilities decrease as the tunneling time increases in the whole range of the observed time. For the higher-order laser beam, Hermite-Gaussian (HG) and Laguerre-Gaussian (LG) the influence of pulse shape on the probabilities, $P^{(1)}_{HG}$, $P^{(1)}_{LG(SP)}$ (dot and dashed line), obtained by a combination of Eq. (15) with Eqs. (25) and (26), respectively, are clearly noticeable (Fig. 3a and 3b). At a fixed laser intensity 4.2×10^{14} W/cm^2 $P^{(1)}_{HG}$ has an approximately three times lower value than $P^{(1)}_{LG(SP)}$. The probability $P^{(1)}_{HG}$ is possible when the tunneling time is in the range of $t = (1 - 150)$ as

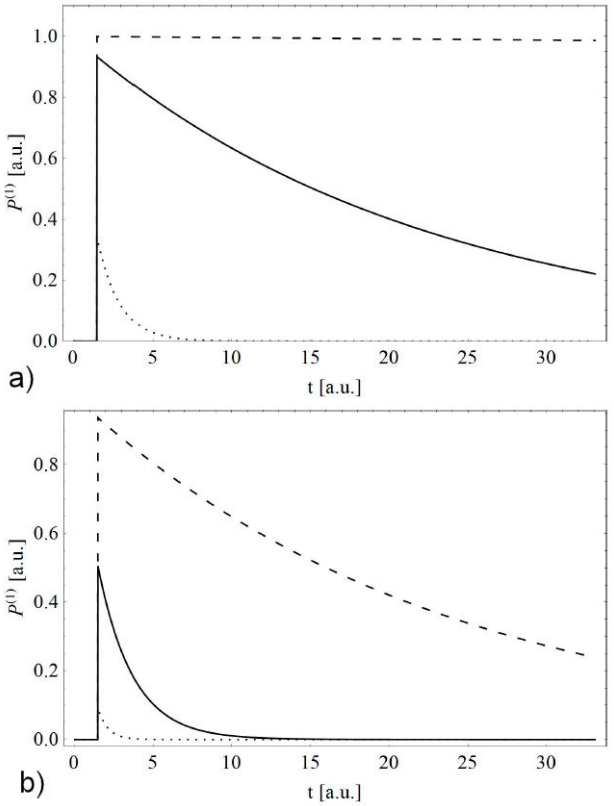

FIGURE 3. Exponential probability distribution as a function of the tunneling time. $P^{(1)}_G$, $P^{(1)}_{SG}$ (beam order $n = 4$), $P^{(1)}_L$, (solid line), $P^{(1)}_{HG}$ (dotted line), $P^{(1)}_{LG(SP)}$(dashed line). Tunneling time is in range of $t = (1 - 800)$ as with corresponding value in atomic units $t = (0.041 - 33.073)$a.u. laser intensity is fixed a) at $I = 4.2 \times 10^{14}$ W/cm^2, b) at $I = 1.5 \times 10^{15}$ W/cm^2.

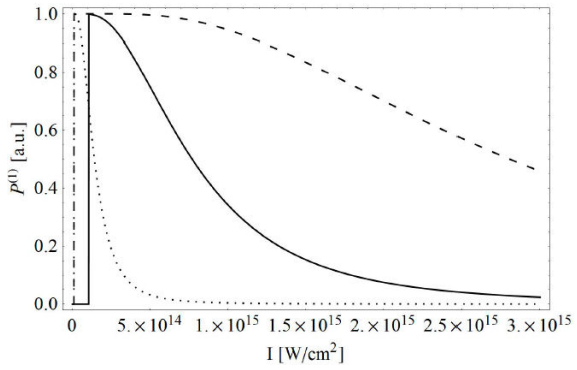

FIGURE 4. Exponential probability distributions. $P_G^{(1)}$, $P_{SG}^{(1)}$ (beam order $n = 4$), $P_L^{(1)}$ (solid line), $P_{HG}^{(1)}$ (dotted line), $P_{LG(SP)}^{(1)}$ (dashed line) vs laser intensity in range $I = (10^{14} - 3 \times 10^{15})$ W/cm^2 for fixed value of tunneling time $t = 100$ as $(4.13$ a.u.$)$.

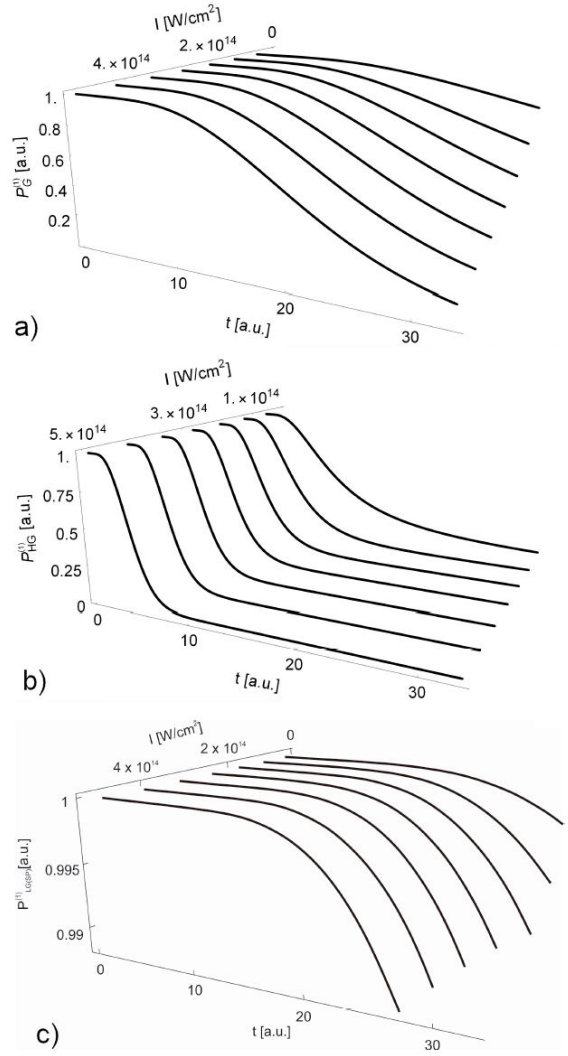

FIGURE 5. Exponential probability distributions $P_G^{(1)}$, $P_{HG}^{(1)}$, $P_{LG(SP)}^{(1)}$ 2D curves plotted into the 3D coordinate system for the intensity range $I = (10^{14} - 5 \times 10^{14})$ W/cm^2 and tunneling time $t = (1 - 800)$ as.

$((0.041 - 6.201)$ a.u.). For $P_{LG(SP)}^{(1)}$ the probability of tunneling is the maximum no matter how long the tunneling time lasts (Fig. 3a). At a stronger field intensity of 1.5×10^{15} W/cm^2 , it is observed that probabilities for all beam profiles decrease with increasing tunneling time (Fig. 3b)). For $P_{HG}^{(1)}$ the tunneling time narrowed in an interval of $(35 - 80)$ as $((1.43 - 3.03)$ a.u.) while $P_{LG(SP)}^{(1)}$ decreases but the tunneling time is still in a wide range.

For the tunneling time $t = 100$ as the probability distribution $P_{G,SG,L}^{(1)}$ (solid line) is the highest at 0.3×10^{14} W/cm^2 (Fig. 4). $P_{HG}^{(1)}$ and $P_{LG(SP)}^{(1)}$ reached a maximum at $I = 0.1 \times 10^{14}$ W/cm^2 and then the $P_{HG}^{(1)}$ probability decreased and at the intensity value 5.5×10^{14} W/cm^2 asymptotically tends to zero. The $P_{LG(SP)}^{(1)}$ probability slightly begins to decrease at the intensity 1.15×10^{14} W/cm^2 and asymptotically tended to zero at higher intensities $\approx 10^{16}$ W/cm^2. Simultaneous dependence probability distributions of laser field intensity and tunneling time, are shown in the 3D coordinate system (Fig. 5).

Tunneling time duration intervals differ from profile to profile of the laser beam (Fig. 5). The shortest time interval gives the HG beam profile and $P_{HG}^{(1)}$ shows the fastest asymptotical tend to zero in the region of the longer tunneling time interval.

3.2. Non-exponential mode

In order to get a basic insight into the tunnel ionization process in a non-exponential regime, calculations analogous to the previous analysis were performed. For inception, the non-exponential probability distribution (Eq. (22)) for the basic form of laser field distribution was calculated. In contrast to the exponential mode, the maximum probability distribution reached much lower values at higher laser intensities. In Fig. 6a the ionization probability distribution $P_{\text{Basic}}^{(2)}$ 2D curves plotted into a 3D coordinate system is obtained as a function of the tunneling time ($t = (1 - 800)$ as) and concrete values of laser intensities: $(4.0 \times 10^{14}, 7.0 \times 10^{14}, 9.0 \times 10^{14}, 1.3 \times 10^{15}, 1.5 \times 10^{15}, 1.75 \times 10^{15}, 2.0 \times 10^{15})$ W/cm^2. It can clearly be seen that the position of the peak does not change, but reached maximum values decrease with increasing field values. The tunneling time interval narrows from $t = (1 - 500)$ as to instantaneous tunneling at higher laser intensities. The laser field is stronger so the potential barrier is suppressed and the electron needs a shorter time to pass through. Using the 3D surface plotting method, in a wide range of laser field intensity and full interval of tunneling time, a more complete picture of the ionization probability $P_{\text{Basic}}^{(2)}$ behavior is obtained. A steep drop with a long plateau was observed (Fig. 6b).

Assuming how long the tunneling time can last, the probability distribution dependence on the intensity of the laser field was analyzed Fig. 7. As the tunneling time increases, the non-exponential probability distribution decreases. The

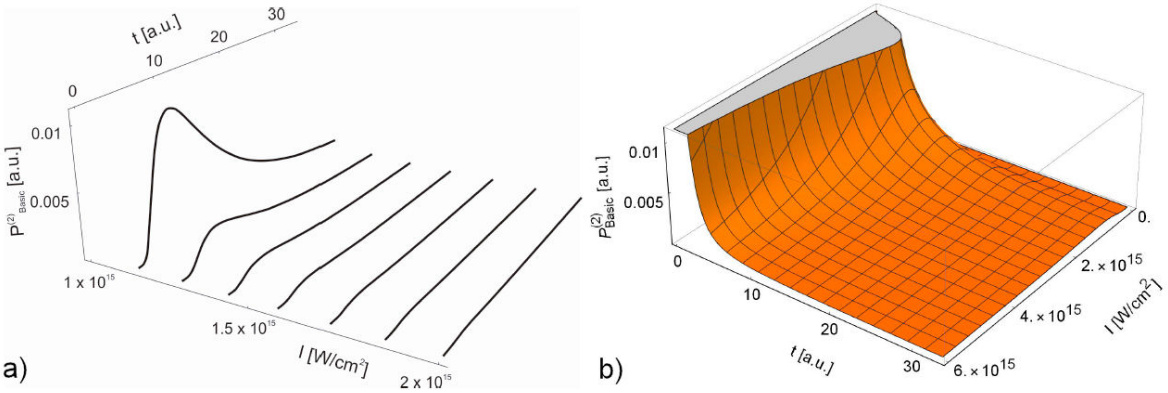

FIGURE 6. Non-exponential probability distribution $P^{(2)}_{Basic}$, as a function of tunneling time in the interval $t = (1 - 800)$ as and laser intensity range: a) $I = (10^{15} - 2 \times 10^{15})$ W/cm^2, b) $I = (10^{15} - 6 \times 10^{15})$ W/cm^2.

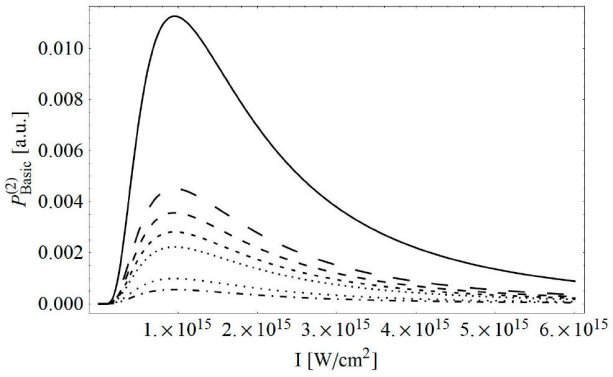

FIGURE 7. Non-exponential probability distribution $P^{(2)}_{\text{Basic}}$, for the laser intensity range $I = (8 \times 10^{14} - 6 \times 10^{15})$ W/cm^2. Each probability curve corresponds to an integer value of attoseconds of tunneling time. $t_1 = 1$as (solid line), $t_2 = 50$as (large dashed line), $t_3 = 100$ as (medium dashed line), $t_4 = 200$ as (small dashed line), $t_5 = 400$ as (tiny dashed line), $t_6 = 600$ as (dotted line), $t_7 = 800$ as (dot-dashed line).

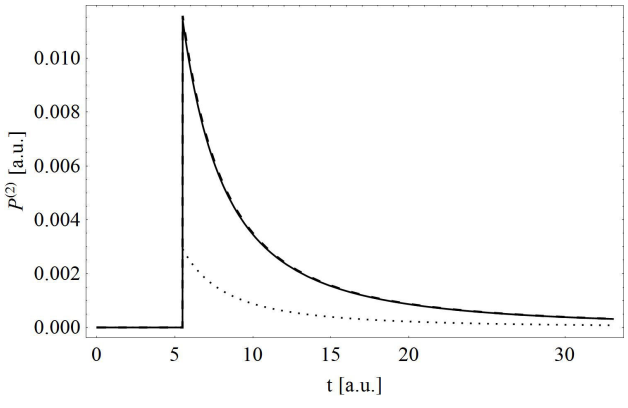

FIGURE 8. Non-exponential probability distribution $P^{(2)}_G$, $P^{(2)}_{SG}$ (beam order $n = 4$), $P^{(2)}_L$ (solid line), $P^{(2)}_{HG}$ (dotted line), $P^{(2)}_{LG(SP)}$ (dashed line) as a function of tunneling time in range of $t = (1 - 800)$ as for fixed value of laser intensity at $I = 1.2 \times 10^{15}$ W/cm^2.

maxima shift to the left, towards lower intensities, which corresponds to a larger barrier width.

We have computed the probability distributions by combining Eqs. (23-27), with Eq. (22) and present them in Fig. 8. It is shown that $P^{(2)}_{\text{Non-exponential}}$ is completely independent of most laser beam profiles. For a fixed laser intensity 1.2×10^{15} W/cm^2, all probability distributions overlapped perfectly except $P^{(2)}_{HG}$. The $P^{(2)}_{HG}$ probability distribution has a five times lower value and a much narrower time interval in which tunneling is possible. $P^{(2)}_G$, $P^{(2)}_{SG}$, and $P^{(2)}_L$ non-exponential probability distributions reached maximums at a stronger field intensity, compared to the exponential mode, 0.95×10^{15} W/cm^2 (Fig. 9). The positions of maximums define the exit point of the barrier, so it can be seen that this point will be shifted using LG and HG laser beam profiles. The resulting peaks appear at 3.4×10^{15} W/cm^2 and 1.6×10^{14} W/cm^2 intensities of the laser field for $P^{(2)}_{LG(SP)}$ and $P^{(2)}_{HG}$, respectively (Fig. 9).

Variations of the non-exponential probability distribution for the corresponding laser beam profiles, computed following the numerical procedure outlined above, are shown in Fig. 10. In a broad range of tunneling time, $P^{(2)}_G$, $P^{(2)}_{HG}$,

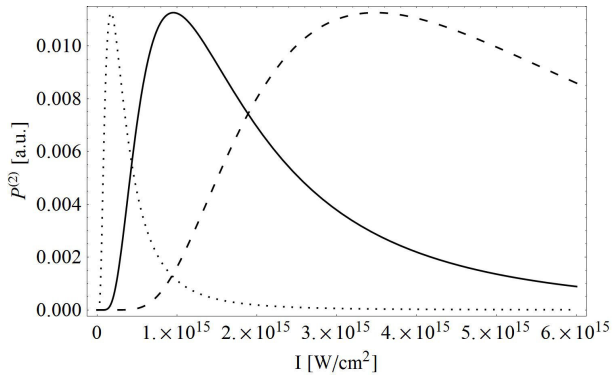

FIGURE 9. Non-exponential probability $P^{(2)}_G$, $P^{(2)}_{SG}$ (beam order $n = 4$.), $P^{(2)}_L$ (solid line), $P^{(2)}_{HG}$ (dotted line), $P^{(2)}_{LG(SP)}$ (dashed line) vs laser intensity in range $I = (8 \times 10^{14} - 6 \times 10^{15})$ W/cm^2 for fixed value of tunneling time $t = 1$ as $(0.0413411$ a.u.$)$.

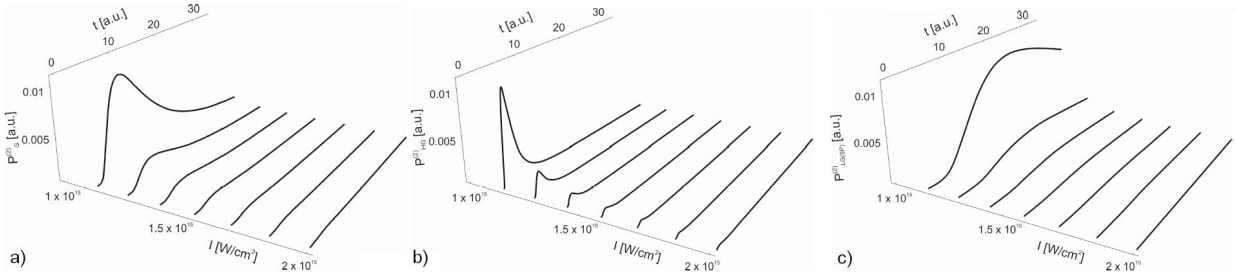

FIGURE 10. Non-exponential probability distributions $P_G^{(2)}$, $P_{HG}^{(2)}$, $P_{LG(SP)}^{(2)}$ 2D curves plotted into a 3D coordinate system for intensity range $I = (10^{15} - 2 \times 10^{15})$ W/cm^2 and tunneling time $t = (1 - 800)$ as.

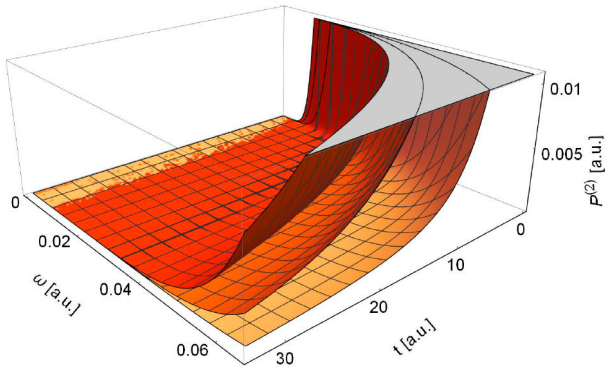

FIGURE 11. Non-exponential probability distributions $P_G^{(2)}$ (red), $P_{LG(SP)}^{(2)}$ (orange), $P_{HG}^{(2)}$ (light orange) vs tunneling time in the interval $t = (1 - 800)$ as and photon energy $\omega = (0.0000456 - 0.0651)$ a.u. which corresponds to the entire infrared spectra $\lambda = (700 \times 10^{-9} - 1 \times 10^{-3})$ m. Laser intensity is fixed at $I = 1.3 \times 10^{15}$ W/cm^2.

$P_{LG(SP)}^{(2)}$ probabilities behave similarly, reach a maximum and then decrease with a long asymmetric tail appearing. Along with an increase of tunneling time, the position of the probability peaks changes. With increasing laser intensity, the maximum values of probabilities become smaller, and at certain field intensities, they are so small that they approach zero.

The analysis is extended into the region of the entire infrared spectrum. Figure 11 presents the results of comparison of the non-exponential probability distribution surfaces $P_G^{(2)}$, $P_{LG(SP)}^{(2)}$, $P_{HG}^{(2)}$, for a fixed laser intensity 1.3×10^{15} W/cm^2. It is observed that the tunnel ionization in the non-exponential domain for these laser beam shapes becomes possible in the region $\omega > 0.04$ a.u. which corresponds to $\lambda > 1.138$ μm.

4. Conclusion

Our paper reported calculation and analysis of the probability distribution of exponential and non-exponential tunneling ionization for the valence electron of a potassium atom exposed to a linearly polarized strong laser field using a broad range of laser intensities. This discussion is presented to investigate the effects of different laser beam profiles that propagate differently and exhibit significantly different spatial distributions on the ionization probability distribution in both modes. Several laser beam profiles were used: fundamental Gaussian and Lorentzian (low-order beams) and Super-Gaussian, Laguerre-Gaussian and Hermite-Gaussian (high-order beams). It was found that application of Gaussian, Lorentzian and Super-Gaussian beam profiles does not affect the exponential probability distribution. Moreover, appropriate probabilities matched perfectly and gave the same tunneling time interval on any laser intensity in the observed range. In the case of Laguerre-Gaussian and Hermite-Gaussian beam profiles, the tunneling time interval is completely different. The probability distribution for the LG profile has a maximum in a large range of tunneling times. On the other hand, the HG probability, for the same parameters, has lower values while the tunneling time is in a much narrower range. Calculations in the non-exponential mode showed that the probability distributions reached a hundred times lower maximum values at much higher laser intensities than in the exponential mode. In the non-exponential mode, all beam profiles give a broad interval of tunneling time, except in the Hermite-Gaussian case where this interval is constricted. In the region of the infrared spectrum, where $\omega < 0.04$ a.u.($\lambda < 1.138$ μm), non-exponential probability distributions are approximately equal to zero. Non-exponential ionization becomes possible only at higher frequencies. The results presented above indicate that the difference between probabilities, computed for lower and higher-order beam field distributions, could be associated with spatial propagation characteristics of the higher-order beam. The spatial beam pattern of the higher-order modes is preserved during propagation to increase the slope of the spatial electric field at any position along the path.

Acknowledgements

The authors acknowledge funding provided by the University of Kragujevac - Institute for Information Technologies (Agreement No. 451-03-68/2022-14/200378), University of Kragujevac - Faculty of Science (Agreement No. 451-03-68/2022-14/200122) through grants by the Ministry of Education, Science and Technological Development of the Republic of Serbia.

1. S.L. Chin, F. Yergeau, and P. Lavigne, *Tunnel ionisation of Xe in an ultra-intense CO2 laser field ($10^{14}\mathrm{Wcm}^{-2}$) with multiple charge creation*, J. Phys. B: Atom. Mol. Phys. **18** (1985) L213 https://doi.org/10.1088/0022-3700/18/8/001
2. N.G. Kelkar, H.M. Castañeda, and M. Nowakowski, *Quantum time scales in alpha tunneling*, EPL **85** (2009) 20006 https://doi.org/10.1209/0295-5075/85/20006
3. W. Fang, R.A. Zarotiadis, J.O. Richardson, *Revisiting nuclear tunneling in the aqueous ferrous-ferric electron transfer*, Phys. Chem. Chem. Phys. **22** (2020) 10687 https://doi.org/10.1039/C9CP06841D
4. T. Nakamura, R. Yoshino, R. Hobara, S. Hasegawa, and T. Hirah, *Development of a convenient in situ UHV scanning tunneling potentiometry system using a tip holder equipped with current-injection wires*, e-J. Surf. Sci. Nanotech. **14** (2016) 216 https://doi.org/10.1380/ejssnt.2016.216
5. A.Nägelein *et al.*, *Investigation of charge carrier depletion in freestanding nanowires by a multi-probe scanning tunneling microscope*, Nano Res. **11** (2018) 5924 https://doi.org/10.1007/s12274-018-2105-x
6. P. Abedini Sohi, Self-Standing Silicon Nanostructures Fabricated Using Chemical/Electrochemical Technique: Application in Gas Field Ionization Tunneling Sensor, Ph.D. thesis, (Concordia University, 2019) https://spectrum.library.concordia.ca/985317/
7. P. Abedini Sohi, and M. Kahrizi, *Low-voltage gas field ionization tunneling sensor using silicon nanostructures*, IEEE Sensors Journal **18** (2018) 6092 doi:10.1109/JSEN.2018.2846254
8. R.B. Sadeghian, and M. Kahrizi, *A novel gas sensor based on tunneling-field-ionization on whisker-covered gold nanowires*, IEEE Sensors Journal **8** (2008) 161 DOI:10.1109/JSEN.2007.912788
9. S.I. Hwang, S.B. Park, J. Mun, W. Cho, C.H. Nam, T.K. Kim, *Generation of a single-cycle pulse using a two-stage compressor and its temporal characterization using a tunnelling ionization method*, Sci. Rep. **9** (2019) 1613 https://doi.org/10.1038/s41598-018-38220-z
10. W. Cho *et al.*, *Temporal characterization of femtosecond laser pulses using tunneling ionization in the UV, visible, and mid-IR ranges*, Sci. Rep. **9** (2019) 16067 https://doi.org/10.1038/s41598-019-52237-y
11. L.D. Landau and E.M. Lifshitz, Course of Theoretical Physics, Vol. 3: Quantum Mechanics: Non Relativistic Theory (Nauka, Moscow, 1989, Pergamon, Oxford, 1991), pp. 295-296
12. L.V. Keldysh, *Ionization in the field of a strong electromagnetic wave*, Sov. Phys. JETP **20** (1965) 1307 https://inspirehep.net/files/6697e05d52e411291acc8238a780db45
13. T.D.G. Walsh, F.A. Ilkov, J.E. Decker, S.L. Chin, *The tunnel ionization of atoms, diatomic and triatomic molecules using intense 10.6 μm radiation*, J. Phy. B: At. Mol. Opt. Phys. **27** (1994) 3767 DOI:10.1088/0953-4075/27/16/022
14. D.T. Lloyd, K. O'keeffe, and S.M. Hooker, *Comparison of strong-field ionization models in the wavelength-scaling of high harmonic generation*, Opt. Express **27** (2019) 6925 https://doi.org/10.1364/OE.27.006925
15. A.M. Perelomov, V.S. Popov, M.V. Terent'ev, *Ionization of Atoms in an Alternating Electric Field*, Sov. Phys. JETP **23** (1966) 924
16. V.M. Ammosov, N.B. Delone, and V.P. Krainov, *Tunnel ionization of complex atoms and of atomic ions in an alternating electromagnetic field*, Sov. Phys. JETP **64** (1986) 1191
17. R. Romo, A. Hernández, and J. Villavicencio, *Exponential and nonexponential buildup in resonant tunneling*, Phys. Rev. A **87** (2013) 022121 https://doi.org/10.1103/PhysRevA.87.022121
18. A.M. Ishkhanyan, V.P. Krainov, *Non-exponential tunneling ionization of atoms by an intense laser field*, Laser Phys. Lett. **12** (2015) 046002 https://doi.org/10.1088/1612-2011/12/4/046002
19. G. Gamow, *Quantum Theory of the Atomic Nucleus (Zur Quantentheorie des Atomkernes)*, Z. Phys. **51** (1928) 204 https://doi.org/10.1007/BF01343196
20. R.W. Gurney, E.W. Condon, *Quantum mechanics and radioactive disintegration*, Phys. Rev. **33** (1929) 127 https://doi.org/10.1103/PhysRev.33.127
21. L.A. Khalfin, *Contribution to the decay theory of a quasi-stationary state*, Sov. Phys. JETP **6** (1958) 1053
22. C. Rothe, S.I. Hintschich, and A.P. Monkman, *Violation of the Exponential-Decay Law at Long Times*, Phys. Rev. Lett. **96** (2006) 163601 https://link.aps.org/doi/10.1103/PhysRevLett.96.163601
23. S.R. Wilkinson *et al.*, *Experimental evidence for non-exponential decay in quantum tunneling*, Nature **387** (1997) 575
24. C.A. Nicolaides, and D.R. Beck, *On the possibility of observing nonexponential decays in autoionizing states*, Phys. Rev. Lett. **38** (1977) 683 https://doi.org/10.1016/0375-9601(78)90116-0
25. M. Buttiker, and R. Landauer, *Traversal Time for Tunneling*, Phys. Rev. Lett. **49** (1982) 1739 https://link.aps.org/doi/10.1103/PhysRevLett.49.1739
26. H.A. Fertig, *Traversal-Time Distribution and the Uncertainty Principle in Quantum Tunneling*, Phys. Rev. Lett. **65** (1990) 232 https://link.aps.org/doi/10.1103/PhysRevLett.65.2321
27. N. Yamada, *Unified derivation of tunneling times from decoherence functional*, Phys. Rev. Lett. **93** (2004) 170401 https://link.aps.org/doi/10.1103/PhysRevLett.93.170401
28. A.S. Landsman *et al.*, *Ultrafast resolution of tunneling delay time*, Optica **1** (2014) 343 https://doi.org/10.1364/OPTICA.1.000343
29. J. Alda, Laser and Gaussian Beam Propagation and Transformation, (Encyclopedia of Optical Engineering, 2003), pp. 999-1013 DOI:10.1081/E-EOE120009751

30. Z. Liangmin, *Intensity Spatial Profile Analysis of a Gaussian Laser Beam at Its Waist Using an Optical Fiber System*, Chin. Phys. Lett. **27** (2010) 054207 DOI:10.1088/0256-307X/27/5/054207

31. K. Gillen-Christand, G.D. Gillen, M.J. Piotrowicz, M. Saffman, *Comparison of Gaussian and super Gaussian laser beams for addressing atomic qubits*, Appl. Phys. B **122** (2016) 1 https://doi.org/10.1007/s00340-016-6407-y

32. Y. F. Chen, T. M. Huang, C.F. Kao, C. L. Wang, S. C. Wang, *Generation of Hermite-Gaussian modes in fiber-coupled laser-diode End-pumped lasers*, IEEE J. Quantum Electron. **33** (1997) 1025 doi:10.1109/3.585491

33. T. Meyrath, F. Schreck, J. Hanssen, C. Chuu, M. Raizen, *A high frequency optical trap for atoms using Hermite-Gaussian beams*, Opt. Express **13** (2005) 2843 https://doi.org/10.1364/OPEX.13.002843

34. L.R. Hofer, L.W. Jones, J.L. Goedert, R.V. Dragone, *Hermite-Gaussian mode detection via convolution neural networks*, J. Opt. Soc. Am. A **36** (2019) 936 https://doi.org/10.1364/JOSAA.36.000936

35. F. Pampaloni, J. Enderlein, *Gaussian, Hermite-Gaussian, and Laguerre-Gaussian beams: A primer*, arXiv.org (November 2004) Source: https://arxiv.org/abs/physics/0410021arXiv

36. N.K. Fontaine, R. Ryf, H. Chen, D.T. Neilson, K. Kim, J. Carpenter, *Laguerre-Gaussian mode sorter*, Nat. Commun. **10** (2019) 1865 https://doi.org/10.1038/s41467-019-09840-4

37. A. Sainte-Marie, O. Gobert, F. Quere, *Controlling the velocity of ultrashort light pulses in vacuum*, Optica **4** (2017) 1298 https://doi.org/10.1364/OPTICA.4.001298

38. D. J. Armstrong, M. C. Phillips and A.V. Smith, *Generation of radially polarized beams with an image-rotating resonator*, Appl. Opt. **42** (2003) 3550 https://doi.org/10.1364/AO.42.003550

39. G. Machavariani, N. Davidson, Y. Lumer, I. Moshe, A. Meir, S. Jackel, New methods of mode conversion and brightness enhancement in high-power lasers, European Conference on Lasers and Electro-Optics and the International Quantum Electronics Conference (Munich, 2007), pp. 1 doi:10.1109/CLEOE-IQEC.2007.4385831

40. P. Klarskov, A.C. Strikwerda, K. Iwaszczuk, P.U. Jepsen, *Experimental three-dimensional beam profiling and modeling of a terahertz beam generated from a two-color air plasma*, New J. Phys. **15** (2013) 075012 https://doi.org/10.1088/1367-2630/15/7/075012

41. M.F. Ciappina, S.V. Popruzhenko, S.V. Bulanov, T. Ditmire, G. Korn, S. Weber, *Progress toward atomic diagnostics of ultrahigh laser intensities*, Phys. Rev. A **99** (2019) 043405 https://link.aps.org/doi/10.1103/PhysRevA.99.043405

42. M.F. Ciappina, E.E. Peganov, and S.V. Popruzhenko, *Focal-shape effect on the efficiency of the tunnel-ionization probe for extreme laser intensities*, Matter Radiat. at Extremes **5** (2020) 044401 https://doi.org/10.1063/5.0005380

43. L. Fonda, G.C. Ghirardi, and A. Ramini, *Decay theory of unstable quantum systems*, Rep. Prog. Phys **41** (1978) 589 https://doi.org/10.1088/0034-4885/41/4/003

44. M.S. Hosseini, S.A. Alavi, *Breit-Wigner distribution, quantum beats and GSI Anomaly*, Annals of Physics **410** (2019) 167936 https://doi.org/10.1016/j.aop.2019.167936

45. A. Bohm, N.L. Harshman, and H. Walther, *Relating the Lorentzian and exponential: Fermi's approximation, the Fourier transform, and causality*, Phys. Rev. A **66** (2002) 012107 https://link.aps.org/doi/10.1103/PhysRevA.66.012107

46. B. Yang *et al.*, U_p, $3U_p$, $11U_p$*: Above-threshold ionization revisited*, Acta Phys. Pol. A **86** (1994) 41

47. A. Karamatskou, *Nonlinear effects in photoionization over a broad photon-energy range within the TDCIS scheme*, J. Phys. B: At. Mol. Opt. Phys. **50** (2017) 013002 http://dx.doi.org/10.1088/1361-6455/50/1/013002

48. C. Anastopoulos, *Decays of unstable quantum system*, Source: arXiv.org (December 2018) https://arxiv.org/pdf/1808.03798.pdf

49. O. Rosas-Ortiz, N. Fernandez-Garcia, and S. Cruz y Cruz, *A Primer on Resonances in Quantum Mechanics*, Source: arXiv.org (February 2004) https://arxiv.org/pdf/0902.4061.pdf

50. J-F Bisson, *Probability density function of the rate of energy transfer from luminescent ions to a random distribution of traps in the static limit*, J. Opt. Soc. Am. B **32** (2015) 757 http://dx.doi.org/10.1364/JOSAB.32.000757

51. P. Wessels *et al.*, *Absolute strong-field ionization probabilities of ultracold rubidium atoms*, Commun. Phys. **1** (2018) 1 https://doi.org/10.1038/s42005-018-0032-5

52. H.K. Malik and A.K. Malik, *Strong and collimated terahertz radiation by super-Gaussian lasers*, EPL **100** (2012) 45001 https://doi.org/10.1209/0295-5075/100/45001

53. A.E. Siegman, *Hermite-Gaussian functions of complex argument as optical-beam eigenfunctions*, J. Opt. Soc. Am. **63** (1973) 1093 https://doi.org/10.1364/JOSA.63.001093

54. A. Wünsche, *Generalized Gaussian beam solutions of paraxial optics and their connection to a hidden symmetry*, J. Opt. Soc. Am. A **6** (1989) 1320 https://doi.org/10.1364/JOSAA.6.001320

55. P.X. Wang, Y.K. Ho, Ch. X. Tang, W. Wang, *Field structure and electron acceleration in a laser beam of a high-order Hermite-Gaussian mode*, J. Appl. Phys. **101** (2007) 083113 https://doi.org/10.1063/1.2719708

56. N. Shiokawa and E. Tokunaga, *Quasi first-order Hermite Gaussian beam for enhanced sensitivity in Sagnac interferometer photothermal deflection spectroscopy*, Opt. Express **24** (2016) 11961 https://doi.org/10.1364/OE.24.011961

57. I. Kimel and L.R. Elias, *Relations Between Hermite and Laguerre Gaussian Modes*, IEEE J. Quantum Electron. **29** (1993) 2562 DOI:10.1109/3.247715

58. J. Ouyang *et al.*, *Tailored optical vector fields for ultrashort-pulse laser induced complex surface plasmon structuring*, Opt. Express **23** (2015) 12562 https://doi.org/10.1364/OE.23.012562

59. M.E.J. Friese, T.A. Nieminen, N.R. Heckenberg, H. Rubinsztein-Dunlop, *Optical alignment and spinning of laser-trapped microscopic particles*, Nature **394** (1998) 348 https://doi.org/10.1038/28566

60. A.T. O'Neil, I. MacVicar, L. Allen, and M.J. Padgett, *Intrinsic and extrinsic nature of the orbital angular momentum of a light beam*, Phys. Rev. Lett. **88** (2002) 053601 https://link.aps.org/doi/10.1103/PhysRevLett.88.053601

61. G. Machavariani, Y. Lumer, I. Moshe and S. Jackel, *Effect of the spiral phase element on the radial-polarization* $(0,1)^*$*LG beam*, Opt. Commun. **271** (2007) 190 https://doi.org/10.1016/j.optcom.2006.10.013

62. P.K. Patel *et al.*, *Integrated laser-target interaction experiments on the RAL petawatt laser*, Plasma Phys. Control. Fusion **47** (2005) B833 https://doi.org/10.1088/0741-3335/47/12B/S65

63. V. Yanovsky *et al.*, *Ultra-high intensity- 300-TW laser at 0.1 Hz repetition rate*, Opt. Express **16** (2008) 2109 https://doi.org/10.1364/OE.16.002109

64. M. Nakatsutsumi *et al.*, *Space and time resolved measurements of the heating of solids to ten million kelvin by a petawatt laser*, New J. Phys. **10** (2008) 043046 https://doi.org/10.1088/1367-2630/10/4/043046

65. W.J. Waters, B. King, *On beam models and their paraxial approximation*, Laser Phys. **28** (2018) 015003 https://doi.org/10.1088/1555-6611/aa94dc

66. D.L. Shealy, and J.A. Hoffnagle, *Laser beam shaping profiles and propagation*, Appl. Opt. **45** (2006) 5118 https://doi.org/10.1364/AO.45.005118

67. P. Eckle *et al.*, *Attosecond Ionization and Tunneling Delay Time Measurements in Helium*, Science **322** (2008) 1525 https://doi.org/10.1126/science.1163439

68. D. Shafir *et al.*, *Resolving the time when an electron exits a tunnelling barrier*, Nature **485** (2012) 343 https://doi.org/10.1038/nature11025

69. D. Bauer, Theory of Laser-Matter Interaction, Max-Planck Institute (Heidelberg, 2006), pp.56-61

70. A.F. González, Chirped Pulse Oscillators: Generating microjoule femtosecond pulses at megahertz repetition rate, Ph.D. thesis, (Dissertation an der Fakultät für Physik der Ludwig-Maximilians-Universität München, 2007)

71. K-H Hong *et al.*, *100-kHz high-power femtosecond Ti:sapphire laser based on downchirped regenerative amplification*, Opt. Express **14** (2006) 970 https://doi.org/10.1364/OPEX.14.000970

72. A.C. Popescu, M. Ulmeanu, C. Ristoscu, I.N. Mihailescu, *Deposition and surface modification of thin solid structures by high-intensity pulsed laser irradiation, Processes and applications, Woodhead Publishing Series in Electronic and Optical Materials*, Laser Surface Engineering (2015) 287 https://doi.org/10.1016/B978-1-78242-074-3.00012-X

73. A. Pfeiffer *et al.*, *Attoclock reveals natural coordinates of the laser-induced tunnelling current flow in atoms*, Nature Phys. **8** (2012) 76 https://doi.org/10.1038/nphys2125

74. M. Yuan, P. Xin, T. Chu, H. Liu, *Exploring tunneling time by instantaneous ionization rate in strong-field ionization*, Opt. Express **25** (2017) 23493 https://doi.org/10.1364/OE.25.023493

75. N.B. Delone, V.P. Krainov, *Atomic stabilization in a laser field*, Phys. Usp. **38** (1995) 1247 https://doi.org/10.1070/PU1995v038n11ABEH000119